Modeling Dilution Jet Flowfields

J. D. Holdeman*
NASA Lewis Research Center, Cleveland, Ohio
and
R. Srinivasan†
The Garrett Turbine Engine Company, Phoenix, Arizona

This paper compares temperature field measurements from selected experiments on a single row, double rows, and opposed rows of jets injected into a ducted cross flow with profiles calculated using an empirical model based on assumed vertical profile similarity and superposition, and distributions calculated with a three-dimensional elliptic code using a standard k-ϵ turbulence model. The empirical model predictions are very good within the range of the generating experiments and the numerical model results, although exhibiting too little mixing, correctly describe the effects of the principal flow and geometric variables.

Nomenclature

A_j/A_m = jet-to-mainstream area ratio,
= $(\pi/4)/[(S/H_0)(H_0/D)^2]$ for one-side injection,
= $(\pi/2)/[(S/H_0)(H_0/D)^2]$ for two-side injection
C = $(S/H_0)(\sqrt{J})$; see Eq. (3)
C_d = orifice discharge coefficient
D = orifice diameter
D_j = $(D)(\sqrt{C_d})$
DR = jet-to-mainstream density ratio,
= (T_m/T_j)
H_0 = duct height
J = jet-to-mainstream momentum flux ratio,
= $(\mathrm{DR})(R)^2$
M = jet-to-mainstream mass flux ratio,
= $(\mathrm{DR})(R)$
R = jet-to-mainstream velocity ratio,
= (V_j/U_m)
S = spacing between orifice centers
S_x = spacing between orifice rows
T = temperature
T_j = jet exit temperature
T_m = mainstream temperature
U = velocity
U_m = mainstream velocity
V_j = jet velocity
w_j/w_T = jet-to-total mass flow ratio,
= equilibrium θ,

$$= \frac{[\sqrt{(DR)(J)}](C_d)(A_j/A_m)}{1+[\sqrt{(DR)(J)}](C_d)(A_j/A_m)}$$

$W^+_{1/2}$ = jet half-width below the centerline (for top injection); see Fig. 4
$W^-_{1/2}$ = jet half-width above the centerline (for top injection); see Fig. 4
x = downstream coordinate (zero at injection plane)
y = cross-stream (radial) coordinate (zero at injection wall)
= y_c at location of maximum θ in a vertical profile; see Fig. 4
z = lateral (circumferential) coordinate (zero at center plane)
θ = temperature difference ratio,
= $(T_m - T)/(T_m - T_j)$; see Eq. (1)
θ_c = maximum temperature difference ratio in a vertical profile; see Fig. 4
$\theta^+_{\min}$ = minimum temperature difference ratio below the centerline (for top injection); see Fig. 4
$\theta^-_{\min}$ = minimum temperature difference ratio above the centerline (for top injection); see Fig. 4

Presented as Paper 84-1379 at the AIAA/SAE/ASME 20th Joint Propulsion Conference, Cincinnati, Ohio, June 11-13, 1984; received July 15, 1984; revision received July 15, 1985. This paper is declared a work of the U.S. Government and therefore is in the public domain.

*Aerospace Engineer, Modeling and Verification Branch. Member AIAA.
†Senior Engineering Specialist, Combustion Engineering Sciences.

Introduction

CONSIDERATIONS of dilution zone mixing in gas turbine combustion chambers have motivated several studies of the mixing characteristics of single and multiple jets injected into a cross flow in a constant-area duct, e.g., Refs. 1-9. Recently, experimental results have been reported that provide insight into the effect of several geometric and flow variations characteristic of most gas turbine combustion chambers, namely, a variable-temperature mainstream, flow area convergence, double rows of holes, and opposed rows of jets, either in-line or staggered.[10-17]

One factor making investigations of the combustor dilution zone jet-in-a-crossflow different from other studies in the literature is that this application is a confined mixing problem, with 10-50% of the total flow entering through the dilution jets. The result is that the equilibrium temperature of the exiting flow may differ significantly from that of the entering mainstream flow. To control or tailor the combustor exit temperature pattern, it is necessary to be able to characterize the exit distribution in terms of the upstream flow and geometric variables. This requires that the entire flowfield be either known or modeled.

From the data of Refs. 1, 11, 14, and 17, an empirical model was developed[4,5] and extended[11,14,17] for predicting the temperature field downstream of a single row, double rows, or opposed rows of jets mixing with a confined cross flow. An interactive microcomputer program (Apple DOS 3.3), based on the model of Ref. 5, was used in Ref. 9 to study the effects of separately varying the independent flow and geometric parameters and to identify the key variables and the relationships among them that characterize the mixing.

Empirical correlation of experimental data can provide a very good predictive capability for the modeled variables within the parameter range of the generating experiments. Also, rapid advances have been made recently in the capability of computational fluid dynamics models and their application

to complex flows such as jet(s) in a cross flow.[18-22] The present paper will compare temperature field measurements from selected cases in Refs. 11, 14, and 17 with distributions calculated using an empirical model based on assumed vertical profile similarity and superposition[11,14,17] and a three-dimensional elliptic code with a standard k-ϵ turbulence model.[21] The results will show the capability (or lack thereof) of the models to predict the effects of the principal flow and geometric variables.

Description of the Flowfield

Figure 1 shows a schematic of the dilution jet flowfield for jet injection from the top wall. The temperature field results are presented in three-dimensional oblique views of the temperature difference ratio θ where

$$\theta = \frac{(T_m - T)}{(T_m - T_j)} \tag{1}$$

A sequence of plots of experimental profiles of this parameter at several locations downstream of the jet injection plane, for single-sided top injection, is shown in Fig. 2. In the three-dimensional plots, the temperature distribution is shown in y-z planes normal to the main flow direction x. The coordinates y and z are, respectively, normal and parallel to the orifice row. All θ distributions are shown over a 25 span in the Z-direction.

Note that the cooler jet fluid is identified by the larger values of the θ parameter (i.e., $\theta = 1$ if the local temperature is equal to the jet temperature and $\theta = 0$ if the local temperature is equal to the mainstream temperature). The equilibrium θ for any configuration is equal to the fraction of the total flow entering through the dilution jets, w_j/w_T.

A schematic of the test rig used in the experiments and the orifice configurations investigated are shown in Fig. 3. The dilution jet mixing characteristics were determined experimentally by measuring the mean temperature and pressure distributions with a vertical rake probe positioned at different axial and lateral stations. The primary independent geometric variables for each orifice configuration are the spacing between adjacent orifices S, the orifice diameter D (for noncircular orifices, this is taken as the diameter of a circle of equal area), and, for double rows, the axial spacing between rows S_x. These are expressed in dimensionless form as the ratio of the orifice spacing to duct height S/H_0, the ratio of the duct height to orifice diameter H_0/D, and the ratio of the axial spacing to the duct height S_x/H_0. Further details of the experiments performed are given in Refs. 1, 2, 5, 11, 13, 14, 16, and 17.

Flowfield Models

Empirical

The empirical model for the temperature field downstream of jets mixing with a confined cross flow is based on the observation that properly nondimensionalized vertical temperature profiles everywhere in the flowfield can be expressed in the following self-similar form[5]:

$$\frac{\theta - \theta^{\pm}_{\min}}{\theta_c - \theta^{\pm}_{\min}} = \exp\frac{-(ln2)(y - y_c)^2}{(W^{\pm}_{1/2})^2} \tag{2}$$

where θ is the local temperature difference ratio defined by Eq. (1) and θ_c, $\theta^{+}_{\min}$, $\theta^{-}_{\min}$, $W^{+}_{1/2}$, $W^{-}_{1/2}$, and Y_c are scaling parameters as shown in Fig. 4. Correlations have been developed for each of these parameters in terms of the independent variables J, S/D, H_0/D, Z/S, and X/H_0. The correlations of Ref. 5 for a single row of jets in a uniform temperature cross flow have been extended for predicting the temperature field downstream of single, double, or opposed rows of jets, either in-line or staggered, injected into an isothermal or nonisothermal mainstream, with and without flow area convergence.[11,14,17]

Numerical

The numerical code used in this investigation is based on the USARTL three-dimensional model[18] and uses pressure and velocities as the main hydrodynamic variables. This code, or similar versions thereof, has been used in previous validation and assessment studies.[19-22]

The governing equations are represented by finite difference approximations on a staggered grid system. The differencing technique employed is hybrid for convective terms; central differencing is used for all other terms. The velocity/pressure coupling is handled by the SIMPLE algorithm of Patankar and Spalding.[23,24] Uniform velocities and mass flow rates were used at all in-flow boundaries. The code contained a conventional k-ϵ turbulence model and standard values of the constants C_D, C_1, and C_2 were used (i.e., $C_D = 0.09$, $C_1 = 1.44$, $C_2 = 1.92$). The rms turbulence intensity was chosen to be 4.5% of the local mean velocity; the inlet length scale was 2% of the jet diameter and duct height for the jet and mainstream, respectively; and the turbulent Schmidt number was 0.9 for all calculations.

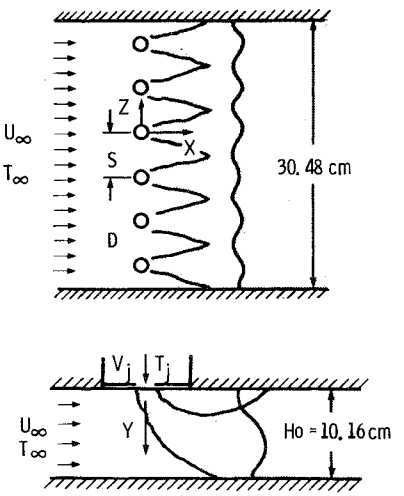

Fig. 1 Schematic of multiple-jet flow.

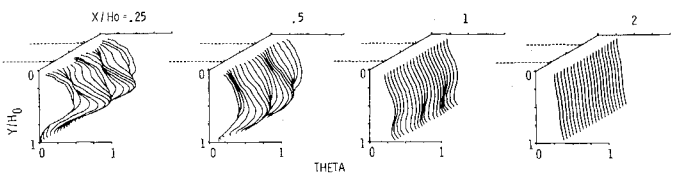

Fig. 2 Experimental mean temperature distributions ($J = 26.2$, $S/H_0 = 0.5$, $H_0/D = 4$).

Table 1 Flow and geometry conditions

Fig.	S/H_0	H_0/D	A_j/A_m	C_d	DR	J	w_j/w_T	C[a]
2	0.5	4.	0.10	0.76	2.2	26.2	0.36	2.56
5a	0.25	8.	0.05	0.60	2.1	22.4	0.17	1.18
5b	1.0	4.	0.05	0.67	2.2	23.5	0.19	4.85
6a	0.5	5.7	0.05	0.71	2.2	25.4	0.21	2.52
6b	0.5	4.	0.10	0.61	2.1	18.6	0.27	2.16
7	0.5	4.	0.10	0.61	1.8	31.3	0.31	2.80
8	0.5	4.[b]	0.10	0.66	2.2	27.1	0.33	2.60
9	0.5	5.7	0.05	0.65	2.2	26.3	0.33	2.56
	0.5	5.7	0.05	0.66	2.2	26.9	—	2.59
10	0.5	5.7	0.05	0.69	2.2	26.8	0.34	2.59
	0.25	8.	0.05	0.70	2.2	26.6	—	1.29
11	0.25	8.	0.10	0.65	2.1	25.0	0.32	1.25
12	1.0	4.	0.10	0.65	2.1	27.6	0.33	5.25

[a] $C = (S/H_0)(\sqrt{J})$. [b] 45 deg slanted slots.

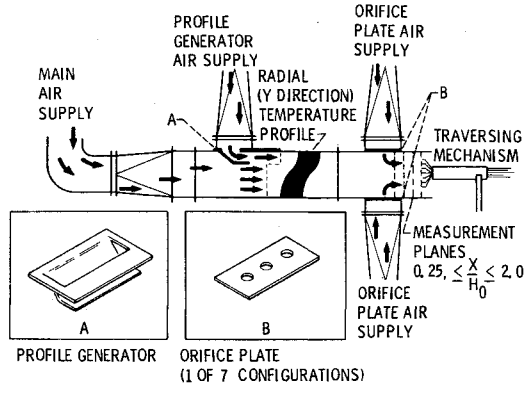

a) Test facility.

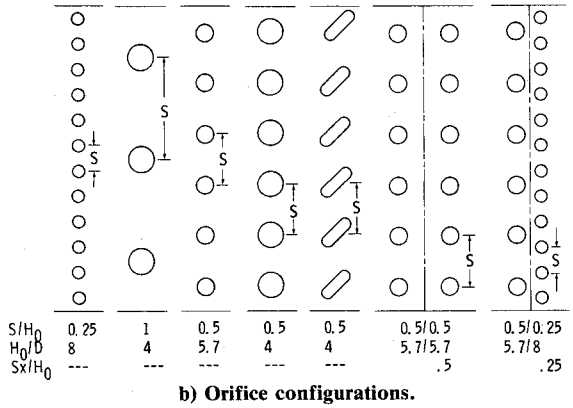

b) Orifice configurations.

Fig. 3 Dilution jet mixing flow and orifice schematic.

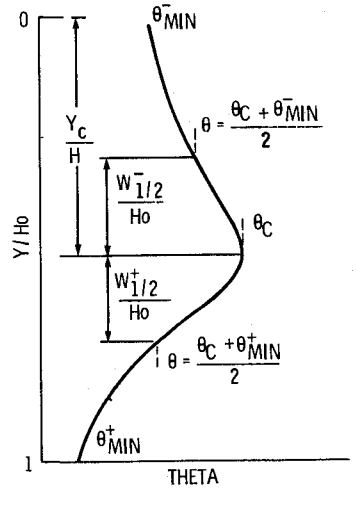

Fig. 4 Schematic of typical vertical temperature profile showing scaling parameters in empirical model.

Results and Discussion

The following paragraphs, and the three-dimensional plots in Figs. 5-12, compare the experimental data with the empirical and numerical model results in the context of the effects of the primary independent variables. The flow and geometry conditions corresponding to these figures are given in Table 1. Isotherm contour plots and center-plane temperature profile plots for most of the conditions examined herein are given in Ref. 15.

Variations with Orifice Size and Spacing

At a constant orifice area, changes in the orifice size and spacing can have a significant influence on the θ profiles. This is shown in Fig. 5, where jets from closely spaced small orifices underpenetrate and remain near the injection wall (part a) and jets from widely spaced larger orifices overpenetrate and impinge on the opposite wall (part b).

The empirical model reproduces the data very well in the small-orifice case, since the data are consistent with the principal assumption in the empirical model—that all vertical temperature distributions can be reduced to similar Gaussian profiles. The empirical model does not do as well in the larger-orifice case, however, as the impingement of the jets on the opposite wall results in vertical profiles that are not similar.

The numerical model calculations made with approximately 20,000 nodes, although in qualitative agreement with the data, show temperature gradients that are too steep, especially in the transverse direction. Underprediction of the mixing was also seen in the single-jet calculations of Ref. 19, where it is shown that the k-ϵ type of turbulence model underestimates the intensity. The result in Fig. 5 is typical of the numerical model calculations to be shown in this paper.

For the small-orifice case, a coarse-grid calculation using less than 6000 nodes was also performed. The numerical results in Fig. 5a illustrate the significant influence of grid selection on the solution obtained and the smearing of the profiles that can occur as a result of numerical diffusion.

Coupled Spacing and Momentum Flux Ratio

Examination of the experimental data revealed that similar jet penetration is obtained over a range of momentum flux ratios, independent of orifice diameter, if orifice spacing and momentum flux ratio are correctly coupled. For example, low momentum flux ratios require large, widely spaced holes, whereas smaller, closely spaced holes are appropriate for high momentum flux ratios.[2,5,9,13]

In general, jet penetration and center-plane profiles are similar when the spacing is inversely proportional to the square root of the momentum flux ratio, i.e.,

$$S/H_0 = C/\sqrt{J} \tag{3}$$

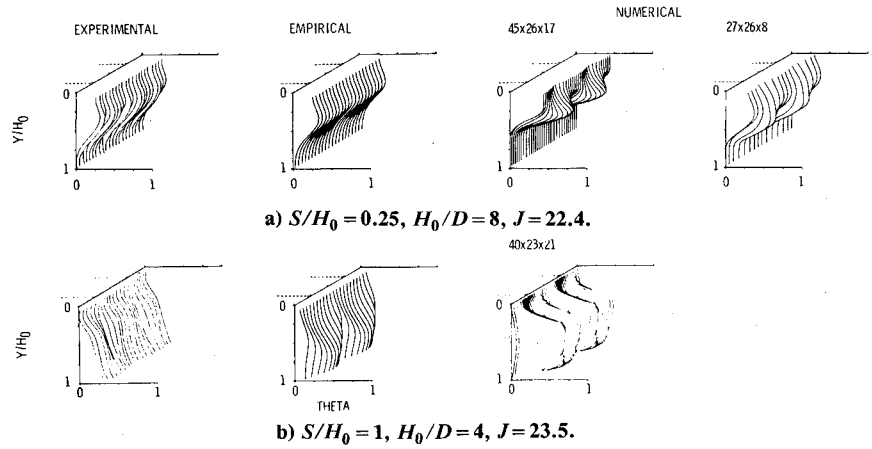

Fig. 5 Effect of varying orifice spacing at constant area on temperature distributions at $X/H_0 = 1$ ($A_j/A_m = 0.05$).

For single-side injection, the center-plane profiles are approximately centered across the duct height and approach an isothermal distribution in the minimum downstream distance when $C=2.5$. This appears to be independent of orifice diameter,[5] as shown in both the calculated and experimental profiles in Fig. 6. Values of C in Eq. (3), which are a factor of ≥ 2 smaller or larger than the optimum, correspond to underpenetration or overpenetration, respectively (e.g., Fig. 5).

In the combinations shown in Figs. 5 and 6, the empirical model results are in very good agreement with the data whenever the data are consistent with the Gaussian profile assumption. The numerical model calculations using approximately 20,000 nodes for these cases show a jet penetration that is in good agreement with the data, but the mixing is otherwise underpredicted, as described previously.

Variable Temperature Mainstream

The influence of a nonisothermal mainstream flow on the profiles for intermediate momentum flux ratios with $S/H_0=0.5$ and $H_0/D=4$ can be seen by comparing Fig. 7 with Figs. 2 and 6b. The shape of the experimental profiles in Fig. 7 suggests modeling them as a superposition of the upstream profile and the corresponding jets-in-an-isothermal-mainstream distribution.[13] The hottest temperature in the mainstream flow was used as T_m in the definition of θ [see Eq. (1)] for this case.

This gives a good approximation, as seen in the empirical model results. The agreement is only first order, however, since with a variable-temperature mainstream there can be cross-stream thermal transport due to the flow of mainstream fluid over and around the jets (and hence to different y locations) and this is not accounted for in superimposing the distributions. This becomes apparent if the local mainstream temperature, $T_m(x,y)$, is used in the definition of θ in Eq. (1).

In the variable-temperature mainstream case in Fig. 7, the numerical model results agree well with the experimental data, especially on the jet center plane, but the transverse mixing is underpredicted, as in the corresponding isothermal mainstream case in Fig. 6b.

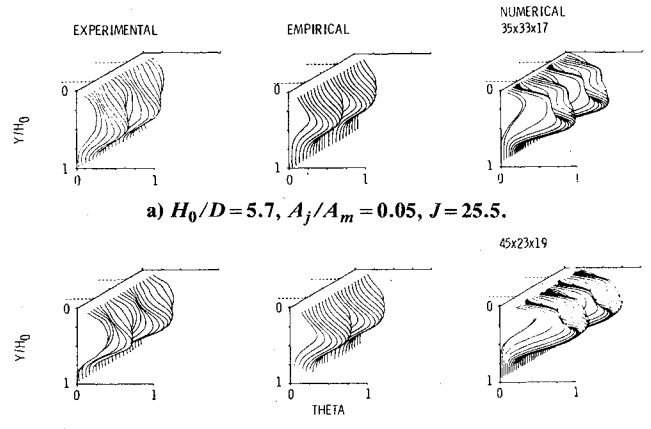

a) $H_0/D=5.7$, $A_j/A_m=0.05$, $J=25.5$.

b) $H_0/D=4$, $A_j/A_m=0.10$, $J=18.6$.

Fig. 6 Effect of varying orifice diameter at constant spacing on temperature distributions at $X/H_0=0.5$ ($S/H_0=0.5$).

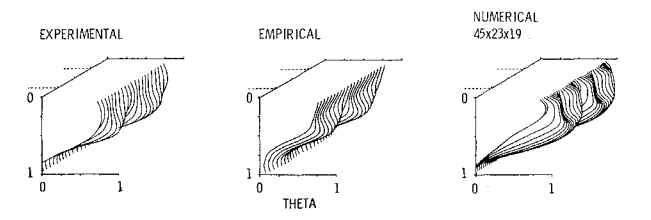

Fig. 7 Temperature distributions at $X/H_0=0.5$ for jets injected into a nonisothermal mainstream; top cold ($S/H_0=0.5$, $H_0/D=4$, $J=31.3$).

Slanted Slots

Figure 8 shows the experimental and calculated temperature distributions at an intermediate momentum flux ratio for a 2.8:1 aspect ratio slot oriented at 45 deg to the main flow direction. The area ratio for this configuration is the same as for the circular holes in Figs. 2 and 6b. As noted in Ref. 16, there does not appear to be any advantage in this configura-

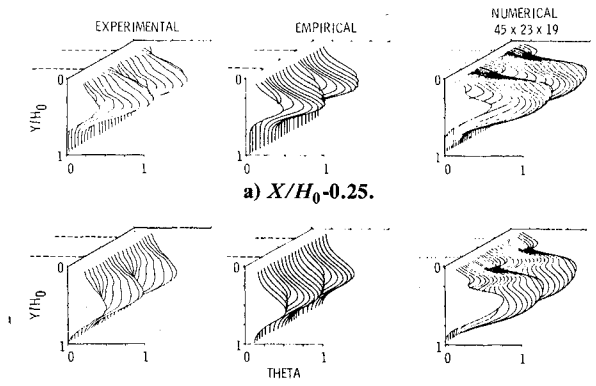

a) X/H_0-0.25.

b) $X/H_0=0.5$.

Fig. 8 Temperature distributions for slanted slots ($S/H_0=0.5$, $H_0/D=4$, $J=27.1$).

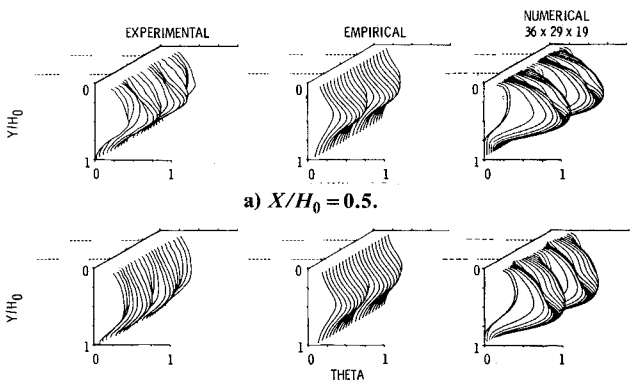

a) $X/H_0=0.5$.

b) $X/H_0=0.75$.

Fig. 9 Temperature distributions for a double row of in-line jets ($A_j/A_m=0.10$, $S_x/H_0=0.5$; row 1: $S/H_0=0.5$, $H_0/D=5.7$, $J=26.3$; row 2: $S/H_0=0.5$, $H_0/D=5.7$, $J=26.9$).

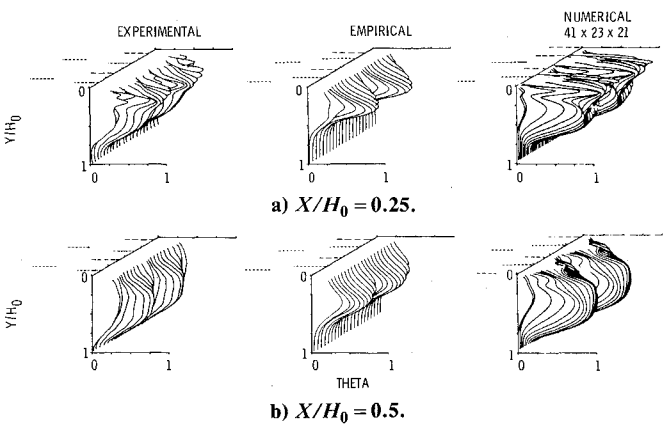

a) $X/H_0=0.25$.

b) $X/H_0=0.5$.

Fig. 10 Temperature distributions for a double row of dissimilar jets ($A_j/A_m=0.10$, $S_x/H_0=0.25$; row 1: $S/H_0=0.5$, $H_0/D=5.7$, $J=26.8$; row 2: $S/H_0=0.25$, $H_0/D=8$, $J=26.6$).

tion compared to circular holes or to streamlined or bluff slots; in fact, the penetration and mixing of the slanted slots are noticeably less. The normally symmetric vortex pair is asymmetric in the case where the slots are slanted with respect to the main flow direction, as is apparent in the experimental profiles in Fig. 8 and the figures in Ref. 16. The experimental profiles also show that the center planes of the jets shift laterally with increasing downstream distance. The empirical model calculations shown in Fig. 8 include this modification, but do not model the asymmetry.[16,17] The numerical calculations for this case exhibit both the center-plane shift and the asymmetry and are good in the context of the qualitative agreement seen throughout the comparisons given in this paper.

Double Rows of Holes

Figure 9 shows experimental and calculated temperature distributions from an orifice plate with two in-line rows of jets ($S_x/H_0=0.5$) from circular orifices. These profiles may be compared with a single row of jets from equally spaced holes in Figs. 2 and 6b. It was observed from the experimental profiles in Refs.1 and 16 that double and single rows have very similar temperature distributions; this is seen in the calculated profiles as well. In this case, the empirical model calculations are derived by superimposing the distributions from independent calculations of the two rows.

Both experimental and calculated temperature distributions are shown in Fig. 10 for a double-row configuration with $S_x/H_0=0.25$, where the trailing row has twice as many orifices as the lead row. Note that the orifice area is the same for both rows. The similarity of these profiles with those from a single row (Fig. 6) and an in-line double row (Fig. 9) is striking, showing the dominance of the lead row in establishing the jet penetration and first-order profile shape.[16] The same conclusion is supported by the empirical and numerical calculations. As with the double row of in-line holes, the empirical calculations for this case were obtained by superimposing separate calculations for the two rows.

Opposed Rows of In-line Jets

For opposed rows of jets of identical orifice spacing and diameter, with the orifice centerlines in-line, the optimum ratio of orifice spacing to duct height is one-half of the optimum value for single-side injection at the same momentum flux ratio.[13] As an example, consider the single-side case with $S/H_0=0.5$ and $H_0/D=4$ in Figs. 2 and 6b and the opposed row of in-line jets with $S/H_0=0.25$ and $H_0/D=8$ in Fig. 11. Note that the product of the spacing and the square root of the momentum flux ratio [C in Eq. (3)] is 1.25 for the latter case, or one-half of the optimum value for single-side injection at this momentum flux ratio.

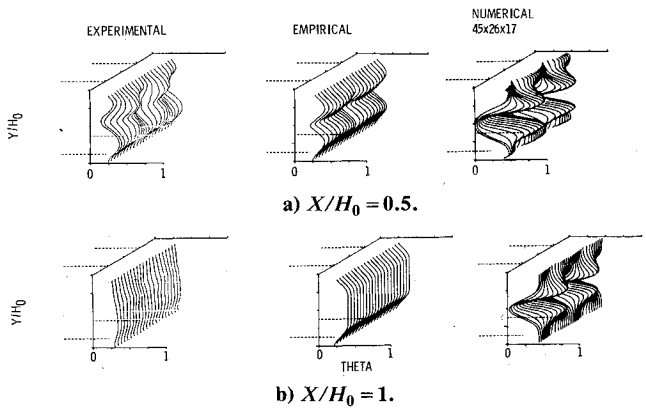

a) $X/H_0=0.5$.

b) $X/H_0=1$.

Fig. 11 Temperature distributions for opposed rows of in-line jets ($S/H_0=0.25$, $H_0/D=8$, $A_j/A_m=0.10$, $J=25$).

The empirical model predicts the opposed-jet case very well, verifying the primary assumption that the effect of a plane of symmetry is similar to that of an opposite wall.[3,9,13] Note that the experimental profiles on both sides of the plane of symmetry support the Gaussian profile assumption. The numerical model results show the steep transverse and lateral gradients that are indicative of too little mixing, as was also seen in almost all of the previous calculations, but the penetration and profile shape are in good agreement with the data.

Opposed Rows of Staggered Jets

For opposed rows of jets of identical orifice spacing and diameter and with the orifice centerlines staggered, the optimum ratio of orifice spacing to duct height is double the optimum value for single-side injection at the same momentum flux ratio.[13] As an example, consider the single-side case with $S/H_0=0.5$ in Fig. 6b [$C=(S/H_0)(\sqrt{J})=2.16$] and the opposed row of staggered jets with $S/H_0=1$ in Fig. 12 ($C=5.25$).

The empirical model does not handle this complex case well, as the fluid dynamic interactions here are not amenable to a direct extension of the simple Gaussian-profile and superposition type of modeling appropriate for most of the single-side and opposed-jet cases of interest. The numerical model calculations are not in appreciably better agreement with the data than the empirical model results, however, as the mixing is underpredicted here as in the previous cases.

As in most of the previous numerical calculations, approximately 20,000 grid points were used, but note that twice as many grid nodes were required in the transverse direction in this case and that the number of axial grid points was correspondingly reduced. The number of axial nodes used in this calculation is approximately the same as that used in the coarse grid calculations shown in Fig. 5a. It follows that the numerical diffusion in the x direction would be comparable between these calculations.

Limitations and Applicability

Empirical

Examination of the empirical model results in this paper shows that correlation of the experimental data can provide a

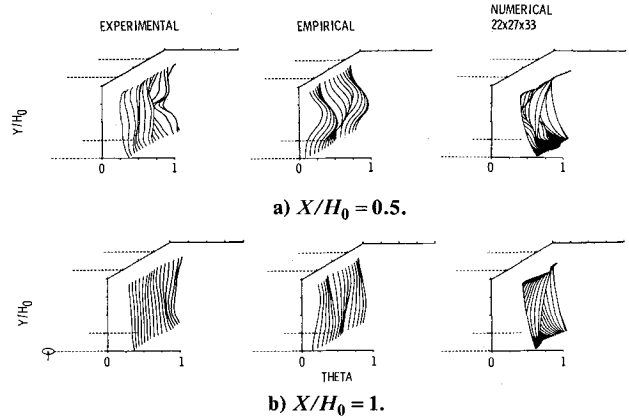

a) $X/H_0=0.5$.

b) $X/H_0=1$.

Fig. 12 Temperature distributions for opposed rows of staggered jets ($S/H_0=1$, $H_0/D=4$, $A_j/A_m=0.10$, $J=27.6$).

Table 2 Range of flow and geometric variables investigated in Refs. 1, 11, 14, and 17

DR	0.5-2.5
J	5-105
S/H_0	0.125-1
H_0/D	4-16
A_j/A_m	0.025-0.1
w_j/w_T	0.075-0.36
$C=(S/H_0)(\sqrt{J})$	0.5-10

good predictive capability within the parameter range of the generating experiments, provided that the experimental results are consistent with the assumptions made in the empirical model. However, these models must be used with caution, or not at all, outside this range.

The range of the experiments on which the empirical model used in this study was based are given in Table 2. The density ratio, momentum flux ratio, orifice spacing, and orifice size were the primary independent variables. The orifice-to-mainstream area ratio, the jet-to-total-mass flow split, and the parameter coupling the spacing and momentum flux ratio, which are derived from the primary variables are also given in the table. Not all combinations of the primary variables in the table were tested—only those combinations that are within the range given for the derived variables represent conditions that are within the range of the experiments.

Considering the results in Figs. 5-12 in the context of Eq. (3) suggests that, in general, the empirical model provides good temperature field predictions for single-side injection when $1<C<5$. Similarly, good predictions are obtained for opposed in-line jets provided that $0.5<C<2.5$. It was shown in Ref. 14 that an opposed row of staggered jets in this range of the parameter C approached, and was satisfactorily modeled with correlations for, the opposed in-line case.

The empirical model does not work well for impinging flows because the experimental temperature distributions are not consistent with the assumption of Gaussian-profile similarity in the empirical model. The experimental profiles for conditions giving optimum mixing in the opposed row staggered-jet configurations are also somewhat at variance with the model assumptions; thus, the satisfactory agreement with the data in these cases must be considered fortuitious. A major weakness of the empirical model used here[11,14,17] (and of the previous versions in Refs. 4 and 5) is that the form of the empirical correlations precludes their use for semiconfined flows (large H_0/D or S/D), single-jet flows, or flows in which it is known a priori that the primary assumptions in the model will be invalid.

Numerical

It is significant to note that the numerical model is not subject to the inherent limitation of the empirical model regarding profile shape and confinement. Thus, three-dimensional codes can provide calculations for complex flows for which the assumptions in the empirical model are known to be invalid or that are outside the range of available experiments. Furthermore, numerical models provide calculations for all flowfield parameters of interest, not just those that happen to have been empirically correlated.

The numerical calculations correctly show the trends that result from the variation in the independent flow and geometric variables, although the results consistently exhibit too little mixing, as seen also in the jet-in-cross-flow calculations using a k-ϵ model reported in Ref. 19. The numerical model calculations for the slanted slots and staggered jet cases are encouraging in that the assumptions in the empirical model are only marginally appropriate for these cases.

The calculations performed are shown to be grid sensitive; thus, numerical, or false, diffusion is known to be present. Uncertainties also exist in these calculations regarding the validity of the turbulence model assumptions and due to unmeasured (and hence assumed) boundary conditions. The results shown here are not intended to represent the "best" agreement possible from numerical models at this time, as better temperature field agreement could undoubtedly have been achieved by adjusting the model constants and/or inlet boundary conditions. Since this was not necessary to satisfy the present objective of evaluating the potential of these codes vis-a-vis combustor dilution zone flowfields and because the mean temperature was the only parameter compared, no such adjustments were made.

Thus, consistent with the previous assessments in Refs. 20-22, three-dimensional calculations such as those in this paper should be considered as only qualitatively accurate at this time. Three-dimensional codes of this type are useful primarily in guiding design changes or in perturbation analyses. The three-dimensional code used herein, although sufficiently promising to justify further development and assessment, is not a practical tool for general engineering use in its present form. Codes with improved numerics, accuracy, and turbulence models should provide more quantitative predictions.

Summary of Results

The present paper compares temperature field measurements from selected experiments, wherein a single row, double rows, or opposed rows of jets were injected into a ducted cross flow, with distributions calculated with an empirical model based on assumed vertical profile similarity and superposition and with a three-dimensional elliptic code using a standard k-ϵ turbulence model.

Empirical model calculations provide very good results for modeled parameters within the range of experiments whenever the primary assumptions are satisfied.

Numerical model calculations can predict all flowfield quantities, flows outside the range of experiments, or flows where empirical assumptions are invalid. Three-dimensional code calculations made in this study correctly approximate the trends that result from variation of the independent flow and geometric variables, but they consistently exhibit too little mixing. Numerical calculations should yield more quantitative predictions with improvements in numerics, accuracy, and turbulence models.

References

[1]Walker, R. E. and Kors, D. L., "Multiple Jet Study Final Report," NASA CR-121217, June 1973.

[2]Holdeman, J. D., Walker, R. E., and Kors, D. L., "Mixing of Multiple Dilution Jets with a Hot Primary Airstream for Gas Turbine Combustors," AIAA Paper 73-1249, Nov. 1973 (also NASA TM X-71426).

[3]Kamotani, Y. and Greber, I., "Experiments on Confined Turbulent Jets in Cross Flow," NASA CR-2392, March 1974.

[4]Walker, R. E. and Eberhardt, R. G., "Multiple Jet Study Data Correlations," NASA CR-134795, April 1975.

[5]Holdeman, J. D. and Walker, R. E., "Mixing of a Row of Jets with a Confined Crossflow," *AIAA Journal*, Vol. 15, Feb. 1977, pp. 243-249 (see also AIAA Paper 76-48, 1976 and NASA TM-71821).

[6]Cox, G. B. Jr., "Multiple Jet Correlations for Gas Turbine Engine Combustor Design," *Journal of Engineering for Power, Transactions of ASME*, Vol. 98, No. 2, 1976, pp. 265-273.

[7]Cox, G. B. Jr., "An Analytical Model for Predicting Exit Temperature Profile from Gas Turbine Engine Annular Combustors," AIAA Paper 75-1307, Sept. 1975.

[8]Khan, Z. A., McGuirk, J. J., and Whitelaw, J. H., "A Row of Jets in Crossflow," *Fluid Dynamics of Jets with Application to V/STOL*, AGARD-CP-308, Technical Editing and Reproduction, London, 1982.

[9]Holdeman, J. D., "Perspectives on the Mixing of a Row of Jets with a Confined Crossflow," AIAA Paper 83-1200, June 1983 (also NASA TM-83457).

[10]Atkinson, K. N., Khan, Z. A., and Whitelaw, J. H., "Experimental Investigation of Opposed Jets Discharging Normally into a Cross-stream," *Journal of Fluid Mechanics*, Vol. 115, 1982, pp. 493-504.

[11]Srinivasan, R., Berenfeld, A., and Mongia, H. C., "Dilution Jet Mixing Phase I Report," Garrett Turbine Engine Co., Phoenix, AZ, Garrett Rept. 21-4302, Nov. 1982 (also NASA CR-168031).

[12]Wittig, S. L. K., Elbahar, O. M. F., and Noll, B. E., "Temperature Profile Development in Turbulent Mixing of Coolant Jets with a Confined Hot Cross-Flow," *Journal of Engineering for Gas Turbines and Power, Transactions of ASME*, Vol. 106, 1984, p. 193 (see also ASME Paper 83-GT-39, 1983).

[13]Holdeman, J. D., Srinivasan, R., and Berenfeld, A., "Experiments in Dilution Jet Mixing," *AIAA Journal*, Vol. 22, Oct.

1984, pp. 1436-1443 (see also AIAA Paper 83-1201, 1983 and NASA TM 83457).

[14]Srinivasan, R., Coleman, E., Johnson K., and Mongia, H. C., "Dilution Jet Mixing Program Phase II Report," Garrett Turbine Engine Co., Phoenix, AZ, Garrett Rept. 21-4804, Dec. 1983 (also NASA CR-174624).

[15]Holdeman, J. D. and Srinivasan, R., "Modeling of Dilution Jet Flowfields," *Combustion Fundamentals Research,* NASA CP-2309, April 1984, pp. 175-187.

[16]Holdeman, J. D., Srinivasan, R., Coleman, E. B., Meyers, G. D., and White, C. D., "Experiments in Dilution Jet Mixing—Effects of Multiple Rows and Non-circular Orifices," AIAA Paper 85-1104, July 1985 (also NASA TM-86996).

[17]Srinivasan, R., Coleman, E., Meyers, G., and White, C., "Dilution Jet Mixing, Phase III Report," Garrett Turbine Engine Company, Phoenix, AZ, Garrett Rept. 21-5418, 1985 (also NASA CR-174884).

[18]Bruce, T. W., Mongia, H. C., and Reynolds, R. S., "Combustor Design Criteria Validation," AiResearch Manufacturing Co. of Arizona, Phoenix, Rept. 75-211682 (38), March 1979 (USARTL-TR-78-55A, B, and C).

[19]Claus, R. W., "Analytical Calculation of a Single Jet in Crossflow and Comparison with Experiment," AIAA Paper 83-0238, Jan. 1983 (also NASA TM-83027).

[20]Sturgess, G. J., "Aerothermal Modeling Phase I Final Report," Pratt & Whitney Aircraft, East Hartford, CT, Rept. PWA-5907-19, May 1983 (also NASA CR-168202).

[21]Srinivasan, R., Reynolds, R., Ball, I., Berry, R., Johnson, K., and Mongia, H. C., "Aerothermal Modeling Program: Phase I Final Report," Garrett Turbine Engine Co., Phoenix, AZ, Garrett Rept. 21-4742, Aug. 1983 (also NASA CR-168243).

[22]Kenworthy, M. J., Correa, S. M., and Burrus, D. L., "Aerothermal Modeling Phase I—Final Report," NASA CR-168296, Nov. 1983.

[23]Patankar, S. V. and Spalding, D. B., "A Calculation Procedure for Heat, Mass, and Momentum Transfer in Three-Dimensional Parabolic Flows," *International Journal of Heat and Mass Transfer,* Vol. 15, Oct. 1972, pp. 1787-1806.

[24]Patankar, S. and Spalding, D., "A Computer Model for Three-Dimensional Flow in Furnaces," *14th Symposium (International) on Combustion,* The Combustion Institute, Pittsburgh, 1973, pp. 605-614.